KSME

Springer

Journal of Mechanical Science and Technology 38 (8) 2024

Original Article
DOI 10.1007/s12206-024-0721-9

Keywords:
· Valveless micropump
· Heating drive
· Couplin
· Pressure

Correspondence to:
Xiaoxiao Yan
qwwxiao@126.com

Citation:
Zhao, S., Wang, X., Zhao, W., Liang, Y., Yan, X., Tang, G., Deng, X., Li, Y. (2024). Simulation and experiment of valveless micropumps driven by piezoelectric–heating coupling for microfluidics. Journal of Mechanical Science and Technology 38 (8) (2024) 4245~4253. http://doi.org/10.1007/s12206-024-0721-9

Received December 20th, 2023
Revised February 27th, 2024
Accepted April 24th, 2024

† Recommended by Editor Chang-Soo Han

Simulation and experiment of valveless micropumps driven by piezoelectric–heating coupling for microfluidics

Shanshan Zhao[1], Xinxin Wang[2], Wenkang Zhao[1], Yanhong Liang[1], Xiaoxiao Yan[1], Gang Tang[1], Xiaozhen Deng[1] and Yuwen Li[1]

[1]Jiangxi Province Key Laboratory of Precision Drive and Control, Nanchang Institute of Technology, Nanchang 330099, China, [2]Jiangsu Sutong Bridge Co, Ltd., Jiangsu, China

Abstract Valveless micropump, important components of a microfluidic system, are widely used in biomedicine, chemical industry, microelectronics cooling and other fields. At present, the driving mode of micropump is mainly single drive, resulting in insufficient driving force and low output pressure. In this study, the overall structure of valveless micropump is designed, and the driving component and the internal inlet and outlet are compared and analyzed by finite element simulation. Moreover, the valveless micropump prototype is processed and developed for performance test. Results show that the output performance of the valveless micropump driven by piezoelectric and heating coupling is better than that of the piezoelectric micropump. When the ambient temperature was 20 °C, 140 V voltage and 40 Hz frequency were added to the piezoelectric component, as well as a 3A current to the heating plate. Furthermore, the liquid flow rate through the microneedle was 0.98 μl/s after a period of time.

1. Introduction

The microfluidic system [1-3] is mainly composed of driving and control components, among which the micropump is the main driving element of the microfluidic system. The micropump integrates the drive source part, pump body, and transmission of the traditional pump [4]; it changes the cavity size through different driving methods to accurately deliver the drug amount. Micropumps can improve the utilization rate of drugs and alleviate the pain caused by their side effects. Nowadays, most micropumps applied in practice include valve pumps, with single drive, large volume, high cost and long-term work. These features not only damage the valve, but also seriously affect the overall performance of the micropump. In addition, residues in the gap between the valve plate and the inlet and outlet are found when the macromolecular liquid is pumped. To solve the many problems caused by valveless micro-pumps, researchers in various countries have carried out a series of studies on valveless micropumps, and examine the different shapes of valveless inlet and outlet [5]. However, a single drive mode of pump under long time work creates many problems, such as insufficient driving force, inaccurate control and slow response.

In recent years, various mechanical micropumps with different driving principles have been developed, including thermal micropumps [6], electrostatic micropumps [7, 8], shape memory alloy micropumps [9-11], electromagnetic micropumps [12, 13], bubble micropumps [14] and piezoelectric micropumps [15-20]. Most of them have complex structures and high-power consumption. Frisk [21] published a research on the production of disposable drug delivery microneedles using an expandable composite of polydimethylsiloxane mix with Expancel® microspheres (PDMS-XB). This pump represents a first step toward transdermal patches for applications that require very precise fluid entry into the skin. Rao [22] proposed a piezoelectric micropump with PDMS as the pump body and Batio3 as the piezoelectric oscillator in 2020. The flow rate of the micropump is most suitable for cardiovascular and hypertension cases. A flow

rate of 854 μl/min was achieved at 50 V voltage drive. In 2020, He [23] proposed a double conical tube valveless piezoelectric (PZT) pump, which has the advantage of higher flow rate than other valve core piezoelectric pumps. The test results show that the driving voltage is 220 V, the frequency is 68 Hz, the pipe diameter is 7 mm, the angle is 20°, the output maximum flow rate is 146.4 ml/min, and the maximum pressure is 520 Pa.

On the basis of this analysis, a valveless micropump with piezoelectric and heating coupling is proposed. The combination of metal thermal drive and piezoelectric plate is used to control the micropump, which can accurately manage the liquid flow of the micropump.

In this study, the structure and dimensions of valveless micropump driver, pump chamber, and inlet and outlet are obtained by theoretical and simulation analysis. Then, different micropumps are manufactured according to the corresponding size. Finally, the performance of valveless micropumps is tested.

2. Design and simulation

2.1 Structure design of micropump

The explosion diagram of the proposed valveless miniature pump designed, which is mainly composed of pump cover, inlet, outlet, piezoelectric plate, base, heating plate, PDMS waterproof film, import and export pipeline, and pump body, is shown in Fig. 1(a). The working principle of the valveless micropump is shown in Figs. 1(b) and (c). Under the given alternating driving voltage, the driver moves up and down and deforms to change the internal volume and pressure of the pump cavity, allowing the liquid to flow. When the driver moves upward, the volume of the pump cavity increases, and the liquid enters the cavity from the inlet and outlet simultaneously because the micropump is valveless. The inlet is a diffusion structure with large end facing inward. The external pressure is large, and the liquid easily flows in, increasing the inflow. However, the small end of the outlet is inward, causing difficulty for the liquid to flow in; thus, the inflow is small. When the driver moves downward, the volume in the pump cavity is reduced, and the liquid is output from the pump inlet and outlet at the same time. However, due to the structural difference between the inlet and outlet, the external pressure at the inlet is greater than that at the outlet, thereby discharging more liquid at the outlet. This micropump can realize the ability of continuously pumping the liquid.

2.2 Driver simulation

2.2.1 Simulation analysis of piezoelectricity

In this section, simulation analysis is conducted according to the simulation modeling method of the piezoelectric oscillator in Wang et al. [24]. The displacement of the piezoelectric plate with different thicknesses is relatively different, affecting the overall performance of the piezoelectric oscillator. Consequently, the performance of the micropump is influenced. In the simulation analysis, the diameter of beryllium bronze base is 18 mm and the thickness is 100 μm, and the diameter of the piezoelectric plate is 14 mm. The applied AC voltage was 200 V, and the results of the piezoelectric sheet with different thicknesses were analyzed, as shown in Fig. 2(a).

The simulation results demonstrate that when the thickness of beryllium bronze is 100 μm and the that of piezoelectric ceramics (PZT-5H) is 150 μm, the maximum center displacement of the piezoelectric oscillator is 57.2 μm. Therefore, the use of beryllium bronze with a thickness of 100 μm and PZT-5 H with a thickness of 150 μm is preferred to fabricate the piezoelectric oscillator. However, in addition to the influence on the performance of the piezoelectric oscillator, the service life and machinability of the piezoelectric oscillator should be considered. Because the thickness of the piezoelectric vibrator cannot be easily processed because it is extremely thin. Moreover, it is susceptible to vibration deformation and easy to fracture, affecting the overall life of the piezoelectric vibrator. Finally, the thickness of bronze and PZT-5 H, which are the most suit-

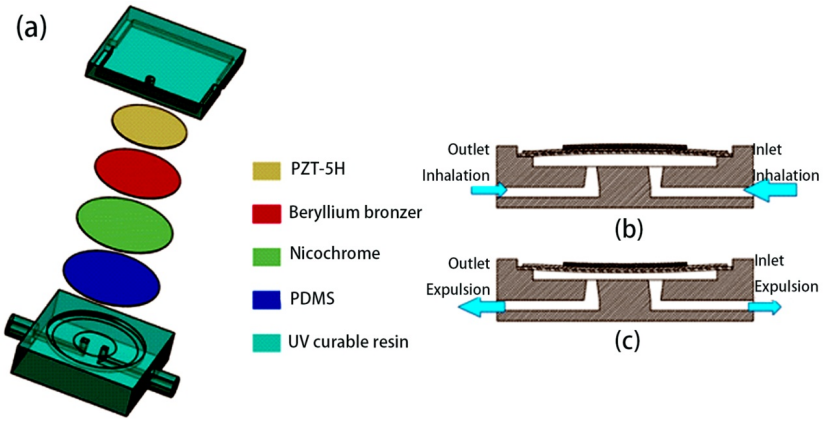

Fig. 1. Overall structure of valveless micropumps: (a) explosion diagram; (b) driver bending upward; (c) driver bends downward and deforms.

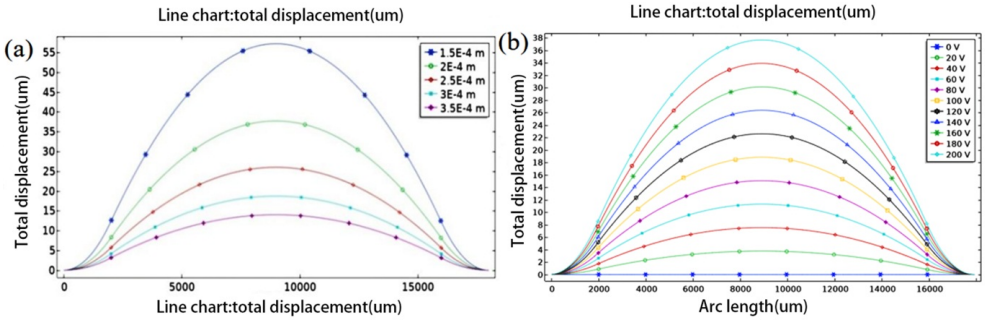

Fig. 2. Piezoelectric simulation: (a) center displacement curves of piezoelectric actuators with different thicknesses; (b) curve of center displacement of piezoelectric oscillator under different driving voltages.

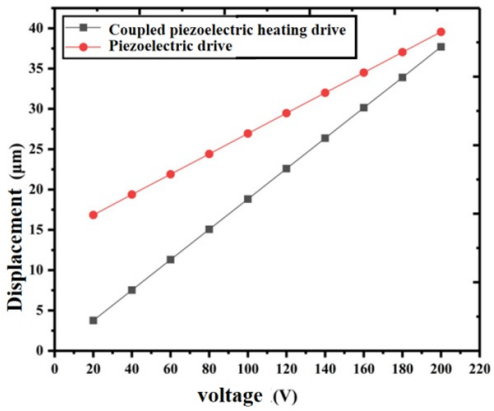

Fig. 3. Displacement curve of piezoelectric/heating coupling displacement under different driving voltages.

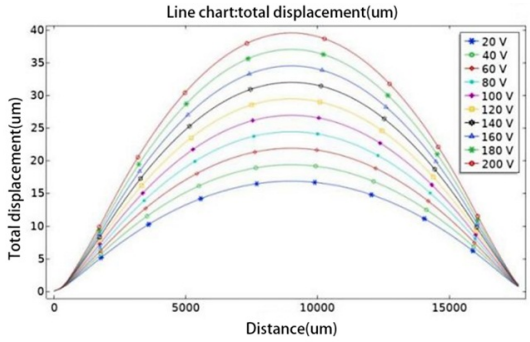

Fig. 4. Comparison of displacement results of piezoelectric and piezoelectric/heating coupling simulation centers.

able piezoelectric vibrators, are set to 100 and 200 μm, respectively. After determining the specific size of the piezoelectric oscillator, different voltages are added to the piezoelectric oscillator for simulation, and the results are shown in Fig. 2(b). The figure shows that the deformation of the piezoelectric oscillator increases with the increase in voltage. The center of the piezoelectric oscillator undergoes the most remarkable change range overall due to the fixed constraints applied. When the voltage is 200 V, the center displacement of the piezoelectric oscillator is 37.7 μm.

2.2.2 Simulation analysis of piezoelectric and heating coupling

In this section, the coupling mode of piezoelectric and heating is simulated and analyzed. The model built in SOLID WORKS2019 was imported into COMSOL5.5 for steady state research, as shown in Fig. 3.

The comparison between Figs. 2(b) and 3 is shown in Fig. 4. The figure illustrates that when a certain current is added to the heating plate, the overall displacement of the driver increases with the increase in partial voltage of the piezoelectric plate, which is slightly larger than that of the piezoelectric drive. The main reason is that when the voltage is added to the piezoelectric oscillator, the displacement of the heating plate is generated when the heating expansion is energized and the relative displacement is generated. The simulation results indicate that the displacement generated by the heating structure is larger than that of the piezoelectric drive, and the relative application in the valveless micropump also increase the liquid pumping capacity of the micropump.

2.3 Import and export simulation

In this study, the circular and prism-shaped inlet and outlet flow channels are designed, and the flow field simulation analysis of these flow channel structures are carried out to find the inlet and outlet structures with the least resistance. In this design, the distance between the import and export centers is set to 2 mm as an example. The import and export of two different structures are simulated under the condition that all parameters and conditions are equal. The results are shown in Figs. 5 and 6. According to the analysis of the flow field diagram and velocity section diagram, the inlet and outlet structures are prism-shaped with relatively flat distribution of streamlines around the inlet and outlet. In addition, streamlines are mostly concentrated near the inlet and outlet, whereas the round-shaped structure has turbulence, sparse distribution of streamlines and serious energy loss. The velocity section diagram also show that the flow velocity direction of the prismatic inlet and outlet flow passage from the inlet to the outlet is consistent with that of the outlet direction, whereas the flow velocity within the round-shaped inlet and outlet passages decreases

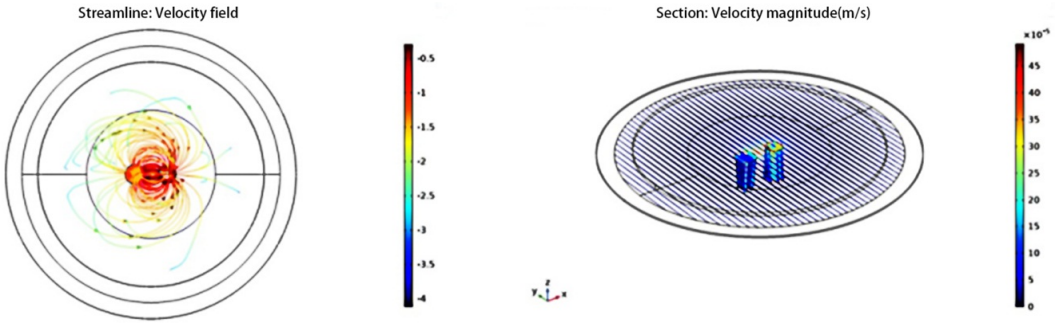

(a) Flow diagram (b) Section diagram

Fig. 5. Round table shape inlet to outlet streamline and velocity section.

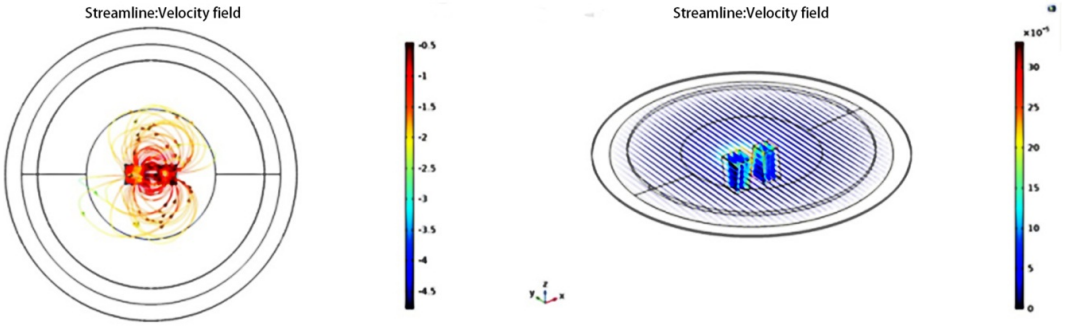

(a) Flow diagram (b) Section diagram

Fig. 6. Prismatic inlet to outlet streamlines and velocity sections.

progressively from the inlet to the outlet, resulting in speed loss. After comprehensive consideration, prismatic inlet and outlet channel are the best options.

3. Production and experiment

Fig. 7 shows the actual valveless micropumps with different inlet and outlet structures. The pump body and cover are processed by 3D printing with SLA technology. The processed material is white photosensitive resin. Each part of the two prototypes has the same size. The actuator of the micropump is made of beryllium bronze with a diameter of 16 mm and a thickness of 0.05 mm. The thickness of piezoelectric chip is 0.2 mm, and the diameter is 14 mm. The heating plate is made of nickel–chromium alloy with a diameter of 18 mm and a thickness of 0.1 mm. Fig. 8 shows the experimental test platform of the valveless micropump. Deionized water is used as the liquid in the test, and different excitations are applied to the driver to measure the output flow and pressure of the valveless micropump. During the test, the mass of the output liquid and the height of the water column were recorded to convert the output flow rate and pressure. The center displacement of the driver is measured by MicrotrakTM3 laser triangle sensor, which is LTS-050-20 produced by MTI Instruments Company, USA. The laser power is less than 5 mW, the response frequency is 0–20 kHz, the sampling frequency is 40 kHz, and the operating temperature is 0–40 °C.

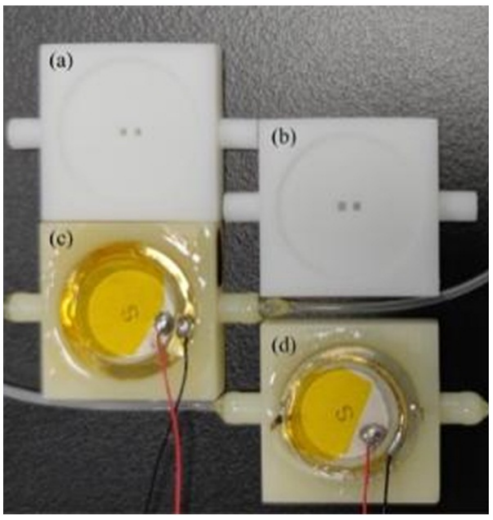

Fig. 7. Valve free micropump: (a) import and export round table micropump; (b) import and export prism micropump; (c) piezoelectric driven micropump; (d) piezoelectric–heating coupling drive micropump.

3.1 Drive displacement characteristic

The piezoelectric driving frequency was fixed at 40 Hz, and 3A current was added to the heating plate. The center displacement of the driver was measured under different voltages added to the piezoelectric, as shown in Fig. 9. The figure illustrates that the displacement of the center of the actuator in-

creases with the increase in the driving voltage of the piezoelectric part, and the linear relationship is excellent. When the driving voltage of the piezoelectric part is 200 V, the displacement of the center of the actuator is 36.9 μm.

3.2 Output flow characteristics of valveless micropump

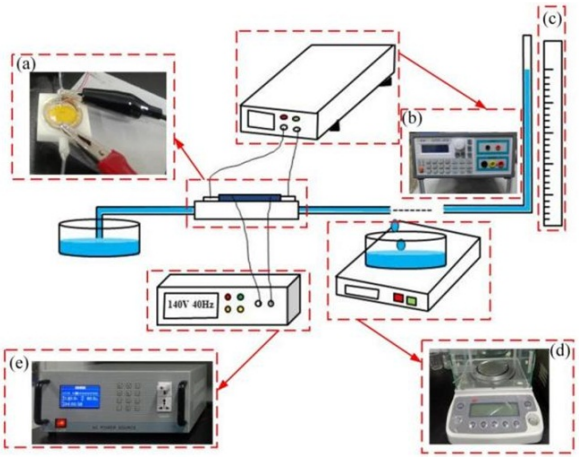

Fig. 8. Performance test platform of valveless micropump: (a) micropump; (b) heating drive power supply; (c) scale; (d) electronic balance; (e) piezoelectric drive power.

Figs. 10(a) and (b) illustrate that under the condition of piezoelectric drive, the flow output at 40 Hz frequency and different voltages of the valveless miniature pump increased continuously with the increase in voltage. At the same time, the output flow of the angular inlet and outlet is larger than that of the circular inlet and outlet, and the maximum output flow can reach 747.9 μl/min when the voltage is 200 V.

Fig. 10(c) shows that when the import and export center distance is farther (6 mm), the output performance is unfavorable,

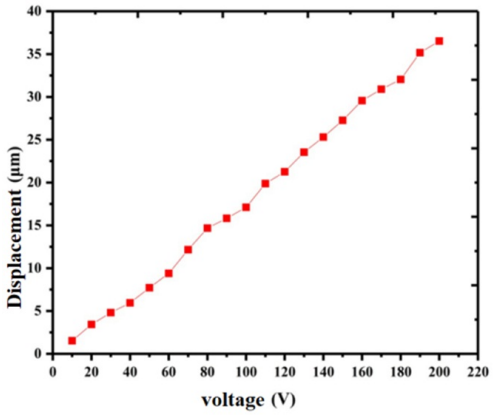

Fig. 9. Driver displacement versus voltage curve.

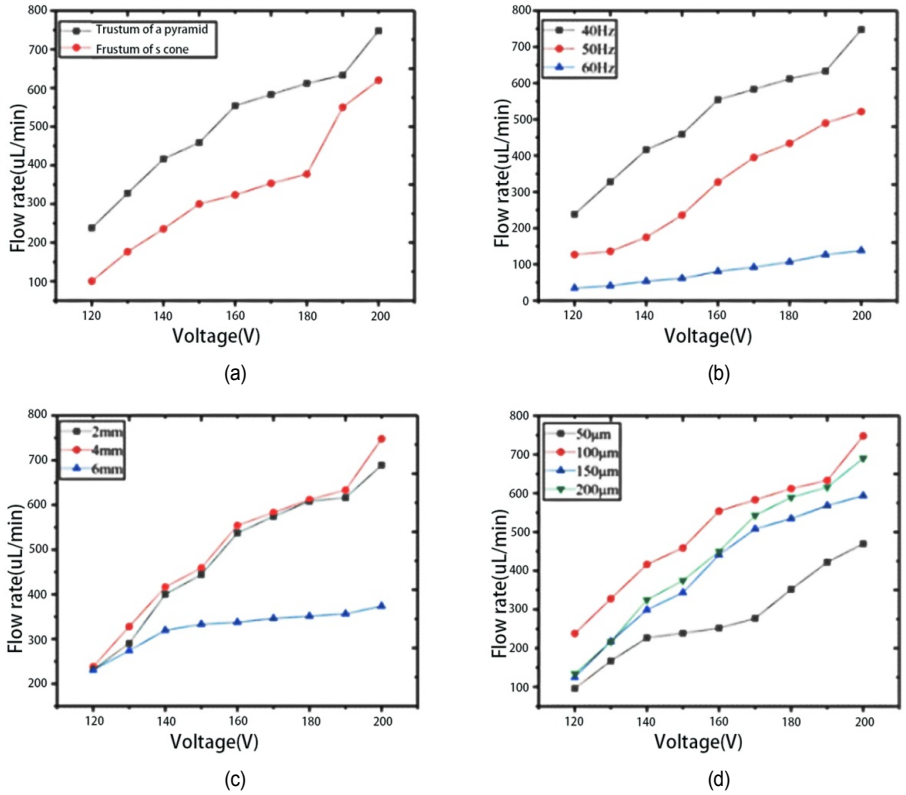

Fig. 10. Relationship between output flow and voltage: (a) output flow of different shapes at inlet and outlet; (b) output flow at different frequencies at inlet and outlet of prism shapes; (c) output flow at different center intervals at the inlet and outlet of prism shape; (d) output flow at different pump cavity heights at the inlet and outlet of prism shape.

due to the proximity of the inlet and outlet to the edge of the pump cavity, the distances from the center of the pump cavity are far from the frequency driven by the piezoelectric vibrator within the first-order frequency. Consequently, the displacement of the center is large, whereas the surrounding displacement is small, leading to lack of driving forces, energy loss and reduced flow output. An extremely close center spacing (2 mm) is mainly due to the phenomenon of reflux in the actual operation of the valveless micropump. The distance between the inlet and outlet is extremely close, resulting in liquid reflux. In addition, a part of the liquid around the pump chamber cannot participate in the liquid flow, easily producing some bubbles and reducing the flow. The results suggest that when the center spacing is 4 mm, the output flow of the valveless micropump is the largest. Considering these tests, the preferred spacing between the import and export centers is 4 mm.

Fig. 10(d) illustrates that at the same frequency, the output flow of the valveless micropump increases gradually with the increase in the applied voltage when the height of the pump chamber increases from 50 μm to 100 μm. Moreover, the output flow is 747.9 μl/min when the maximum voltage is 200 V. When the pump cavity height continued to increase, the output flow rate showed a relatively decreasing trend. When the pump cavity height increased to 200 μm, the output flow rate was 690.4 μl/min. The overall data diagram demonstrate that the output flow of the valveless mini pump increased steadily under the applied voltage of 120 V to 150 V for the four pump chamber heights. The reason for this phenomenon is that when the height of the pump cavity is extremely low, the maximum displacement of the drive movement is extremely large, creating a gap between the liquid and the surrounding liquid in the center of the pump cavity. Consequently, bubbles are easily produced, resulting in a low output flow. When the height of the pump chamber is extremely high, the output liquid is reduced due to the insufficient driving force of the actuator. When the voltage is higher than 150 V, the unstable output liquid flow is caused by the rapid movement of the driver, considering a valveless micropump. The liquid backflows in the pump chamber, resulting in unstable output flow.

3.3 Temperature characteristics of the heating plate

When the ambient temperature is 17 °C, currents 1A, 2A, and 3A are added to the heating sheet. Fig. 11(a) shows that upon the addition of current 3A, the temperature of the heating sheet rises rapidly with the highest temperature reaching 47 °C within 2 minutes. If a large current is continuously added, then the temperature of the heating plate theoretically rises faster, thereby increasing the pressure. However, extremely high temperature causes deformation of the 3D printed pump body, resulting in a gap between the driver and the pump body. This condition leads to air leakage in the pump chamber, affecting the performance of the micropump. Subsequently, when the temperature is extremely high, the liquid in the pump chamber produces bubbles, which block the inlet and outlet and reduce the flow rate. Fig. 11(b) illustrates that after the heating fragment was electrically charged, the surface temperature of the heating piece decreased, and the cooling rate was high. The temperature dropped by 27 °C in 80 s. In conclusion, adding 3A current to the heating plate is more appropriate.

3.4 Comparison of output pressure of valveless micropump with two driving modes

The test results in Fig. 12 show that when the driving voltage is above 90 V, the output pressure of the valveless micropump driven by piezoelectric/heating coupling has an excellent linear relationship with the increase in the driving voltage of the piezoelectric part. When the voltage is 200 V, the maximum output pressure is 588 Pa. When the driving voltage is above 170 V, the output pressure of the valveless micropump driven by piezoelectricity starts to drop due to the valveless backflow. Therefore, the output water column cannot continuously in-

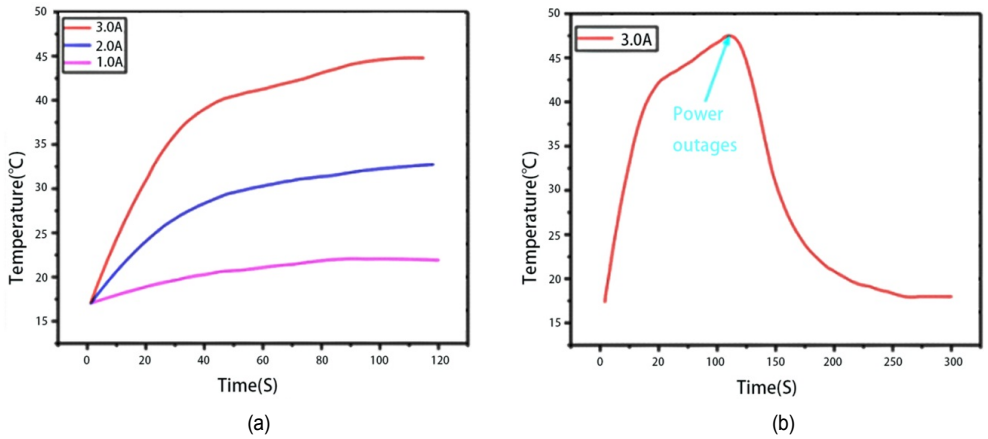

Fig. 11. Curve of temperature change of heating plate with time: (a) temperature change of heating plate with three current types; (b) 3A current is added to the heating plate on and off temperature changes with time.

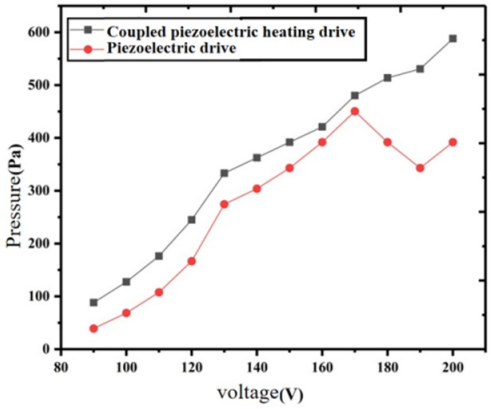

Fig. 12. Comparison of output pressure of two driving modes of micropump with the increase in piezoelectric driving voltage.

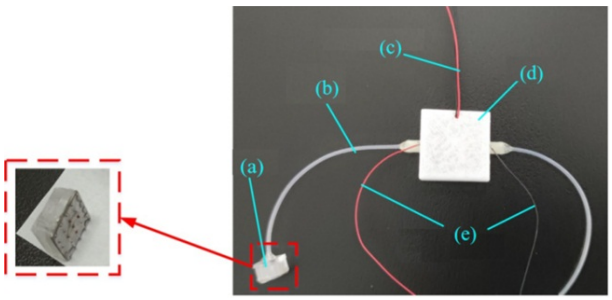

Fig. 13. Valveless micropump combined with microneedle test device: (a) microneedle; (b) pipeline; (c) piezoelectric power supply; (d) micropump; (e) heating power supply.

crease. The output pressure of the micropump driven by piezoelectric/heating coupling can continue to increase when the driving voltage increases because of the power provided by heating. The comparison of the pressure output of the two driving modes suggests that the overall output pressure of the micropump driven by heating coupling is slightly larger than that driven by piezoelectric alone. The heating plate is transferred to the liquid by heat, causing the temperature of the liquid to increase slowly. When the liquid temperature increases, the speed of the irregular movement between molecules is also accelerated, the valve-free micropump chamber and closed container molecular density remain unchanged, and then the number of collisions increases. Consequently, the pressure increases, the force area remains constant, and the pressure naturally increases. Combined with the above analysis, the driver with the heating coupling can increase the output pressure of the valveless micropump.

3.5 Combined with microneedle delivery liquid test

The structure of valveless micropump combined with microneedle for testing is shown in Fig. 13. It is mainly composed of valveless micropump, hose, PDMS drug storage chamber, and microneedle. The connection sequence is as follows: valveless micropump, drug storage chamber and microneedle. They form a continuous drug delivery system under the connection of hose. The microneedle was cut into a needle body by stainless steel, and then a 100 μm micropore was punched in the center of the needle body by laser. The microneedles and PDMS drug storage cavities were initially bonded with photosensitive resin, and then strengthened with Viva 1005 epoxy resin AB glue after curing to prevent leakage at the bonding place. When the ambient temperature was 20 °C, 140 V voltage and 40 Hz frequency were added to the piezoelectric component, and 3A current was added to the heating plate. After a period of time, the flow rate of the liquid through the microneedle was 0.98 μl/s.

4. Conclusion

A coupling method of piezoelectric and heating is proposed to drive the valveless micropump. Through theory and simulation optimization, the optimal size of the actuator is obtained. According to the working principle of diffusion/contraction port, two valveless micropumps with different shapes of the inlet and outlet were designed and simulated by COMSOL software. Finally, a valveless micropump prototype was fabricated, and its output performance was tested. The experimental results show that the output performance of the valveless micropump with heating structure is influenced by the single piezoelectric actuator. In addition, the output pressure of the valveless micropump driven by piezoelectric and heating coupling is approximately 5 % higher than that of the valveless micropump driven by piezoelectric. When the ambient temperature was 20 °C, 140 V voltage and 40 Hz frequency were added to the piezoelectric component, and 3A current was added to the heating plate. After a period of time, the flow rate of the liquid through the microneedle was 0.98 μl/s.

Results of the simulation and experiment suggest that the advantages of the valveless micropump with piezoelectric and heating coupling compared with other micropumps can be obtained. Compared with micropumps with other driving principles (such as electromagnetic micropumps), the drive mode coupled with heating and piezoelectric plates is more stable and relatively simple in structure. Compared with the traditional single piezoelectric plate driving mode, the coupling of metal heater and piezoelectric plate can increase the output pressure, accelerate the drug diffusion, and overcome the difference in the internal and external pressure when the liquid drug enters the organism through the microneedles.

Acknowledgments

This work was partly supported by the National Natural Science Foundation of China (Nos. 62064008) and the Natural Science Foundation of Jiangxi province (Nos. 20202BABL 204041 and GJJ201927). The authors are also grateful to their colleagues for their essential contributions to this work.

References

[1] M. Naseri, G. P. Simon and W. Batchelor, Development of a paper-based microfluidic system for a continuous high-flow-rate fluid manipulation, *Analytical Chemistry*, 92 (10) (2020) 7307-7316.

[2] X. An, P. Zuo and B. C. Ye, A single cell droplet microfluidic system for quantitative determination of food-borne pathogens, *Talanta*, 209 (2020) 120571.

[3] T. Yue, D. Zhao and D. T. T. Phan, A modular microfluidic system based on a multilayered configuration to generate large-scale perfusable microvascular networks, *Microsystems & Nanoengineering*, 7 (1) (2021) 1-13.

[4] F. R. Munas, G. Melroy and C. B. Abeynayake, Development of PZT actuated valveless micropump, *Sensors*, 18 (5) (2018) 1302.

[5] Q. Yan, Y. Yin and W. Sun, Advances in valveless piezoelectric pumps, *Applied Sciences*, 11 (15) (2021) 7061.

[6] B. T. Chia, H. H. Liao and Y. J. Yang, A novel thermo-pneumatic peristaltic micropump with low temperature elevation on working fluid, *Sensors and Actuators A: Physical*, 165 (1) (2011) 86-93.

[7] H. Kim, A. A. Astle and K. Najafi, An integrated electrostatic peristaltic 18-stage gas micropump with active microvalves, *Journal of Microelectromechanical Systems*, 24 (1) (2014) 192-206.

[8] I. Lee, P. Hong and C. Cho, Four-electrode micropump with peristaltic motion, *Sensors and Actuators A: Physical*, 245 (2016) 19-25.

[9] I. Stachiv, E. Alarcon and M. Lamac, Shape memory alloys and polymers for MEMS/NEMS applications: review on recent findings and challenges in design, preparation, and characterization, *Metals*, 11 (3) (2021) 415.

[10] K. Ullakko, L. Wendell and A. Smith, A magnetic shape memory micropump: contact-free, and compatible with PCR and human DNA profiling, *Smart Materials and Structures*, 21 (11) (2012) 115020.

[11] A. Saren, A. R. Smith and K. Ullakko, Integratable magnetic shape memory micropump for high-pressure, precision microfluidic applications, *Microfluidics and Nanofluidics*, 22 (4) (2018) 1-10.

[12] P. Kawun, S. Leahy and Y. Lai, A thin PDMS nozzle/diffuser micropump for biomedical applications, *Sensors and Actuators A: Physical*, 249 (2016) 149-154.

[13] C. Wang, S. J. Seo and J. S. Kim, Intravitreal implantable magnetic micropump for on-demand VEGFR-targeted drug delivery, *Journal of Controlled Release*, 283 (2018) 105-112.

[14] Y. Qu, K. Zhou and W. Wu, Theoretical and experimental research on bubble actuated micro-pumps, *Micromachines*, 9 (5) (2018) 225.

[15] C. H. Cheng, A. S. Yang and C. J. Lin, Characteristic studies of a novel piezoelectric impedance micropump, *Microsystem Technologies*, 23 (6) (2017) 1709-1717.

[16] H. K. Ma, R. H. Chen and N. S. Yu, A miniature circular pump with a piezoelectric bimorph and a disposable chamber for biomedical applications, *Sensors and Actuators A: Physical*, 251 (2016) 108-118.

[17] S. Chen, X. Xie and J. Kan, A hydraulic-driven piezoelectric pump with separable channel for drug delivery, *Sensors and Actuators A: Physical*, 295 (2019) 210-216.

[18] J. Li, H. Huang and T. Morita, Stepping piezoelectric actuators with large working stroke for nano-positioning systems: a review, *Sensors and Actuators A: Physical*, 292 (2019) 39-51.

[19] Z. Zhang, S. Chen and S. Wang, Performance evaluation and comparison of a serial–parallel hybrid multichamber piezoelectric pump, *Journal of Intelligent Material Systems and Structures*, 29 (9) (2018) 1995-2007.

[20] R. K. Haldkar, V. K. Gupta and T. Sheorey, Modeling and flow analysis of piezoelectric based micropump with various shapes of microneedle, *Journal of Mechanical Science and Technology*, 31 (6) (2017) 2933-2941.

[21] T. Frisk, N. Roxhed and G. Stemme, MEMS for medical technology applications, *Microfluidics, BioMEMS, and Medical Microsystems V*, 6465 (2007) 646513.

[22] K. S. Rao, G. V. Ganesh and G. S. Lakshmi, Analysis of PDMS based MEMS device for drug delivery systems, *Microsystem Technologies*, 27 (3) (2021) 659-664.

[23] L. He, X. Wu and D. Hu, Research on output performance of valve-less piezoelectric pump with multi-cone-shaped tubes, *Microsystem Technologies*, 27 (2020) 2091-2102.

[24] X. Wang, S. Zhao and X. Yan, Research on valveless piezoelectric micropump based on COMSOL and 3D printing technology, *Journal of Physics: Conference Series. IOP Publishing*, 2218 (1) (2022) 012073.

Shanshan Zhao received her Master's degree from Nanchang Institute of Technology. Her research interests include MEMS medical devices and microneedle transdermal drug delivery technique.

Wenkang Zhao is a graduate from the School of Mechanical Engineering at Nanchang Institute of Technology. His research interests include MEMS medical devices and promoting drug delivery research.

Xiaoxiao Yan is an Associate Professor in the School of Mechanical Engineering at Nanchang Institute of Technology. He received his Ph.D. in Microelectronics and Solid-state Electronics from Shanghai Jiao Tong University. His research interests include MEMS medical devices and MEMS processes.

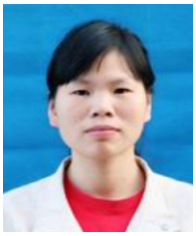

Xiaozhen Deng is an Associate Professor in the School of Mechanical Engineering at Nanchang Institute of Technology. She received her Ph.D. in Mechanical Design and Theory from Nanchang University. Her research interests include new technologies for polymer molding and MEMS technology.

Gang Tang is a Professor and Dean of the School of Mechanics at Nanchang Institute of Technology. He received his Ph.D. in Mechanical Engineering from Shanghai Jiao Tong University. His research interests include microenergy technology, smart sensors and actuators, and MEMS technology.

Yuwen Li is with the School of Electrical Engineering at Nanchang Institute of Technology. She received the M.S. degree in Instrument Science and Engineering from Nanchang University. Currently, she is pursuing a Ph.D. degree at the School of Machinery and Automation, Wuhan University of Science and Technology. Her research interests include medical imaging and machine learning.